Available online at www.sciencedirect.com
SCIENCE DIRECT®
Journal of Sound and Vibration 284 (2005) 531–549
JOURNAL OF SOUND AND VIBRATION
www.elsevier.com/locate/jsvi

Temperature dependent vibration analysis of functionally graded rectangular plates

Young-Wann Kim

Department of Mechanical Engineering, Yosu National University, San 96-1, Dunduck-Dong Yosu, Chonnam, 550-749, Republic of Korea

Received 14 April 2003; received in revised form 7 May 2004; accepted 21 June 2004
Available online 10 December 2004

Abstract

A theoretical method is developed to investigate vibration characteristics of initially stressed functionally graded rectangular plates made up of metal and ceramic in thermal environment. The temperature is assumed to be constant in the plane of the plate and to vary in the thickness direction only. Two types of thermal condition are considered. The first type is that one value of the temperature is imposed on the upper surface and the other (or same) value on the lower surface. The second is that the heat flows from the upper surface to the lower one held at a prescribed temperature. Material properties are assumed to be temperature dependent, and vary continuously through the thickness according to a power law distribution in terms of the volume fraction of the constituents. The third-order shear deformation plate theory to account for rotary inertia and transverse shear strains is adopted to formulate the theoretical model. The Rayleigh–Ritz procedure is applied to obtain the frequency equation. The analysis is based on an expansion of the displacements in the double Fourier series that satisfy the boundary conditions. The effect of material compositions, plate geometry, and temperature fields on the vibration characteristics is examined. The present theoretical results are verified by comparing with those in literature.

E-mail address: ywkim@yosu.ac.kr (Y.-W. Kim).

0022-460X/$ - see front matter © 2004 Elsevier Ltd. All rights reserved.
doi:10.1016/j.jsv.2004.06.043

1. Introduction

Functionally graded materials (FGMs) are composite materials intentionally designed so that they possess desirable properties for specific applications, especially for aircrafts, space vehicles and other engineering structures under high-temperature environment. FGMs are heterogeneous composite materials, in which the material properties vary continuously from one interface to the other. Those are achieved by gradually varying volume fraction of constituent materials. The advantage of using these materials is that they can survive the high thermal gradient environment, while maintaining their structural integrity. FGMs were initially designed as thermal barrier materials for aerospace structural applications and fusion reactors. Now they are developed for the general use as structural components in high-temperature environment.

Typically, an FGM is made of a ceramic and a metal for the purpose of thermal protection against large temperature gradients. The ceramic material provides the high-temperature resistance due to its low thermal conductivity, while the ductile metal constituent prevents fracture due to its greater toughness. Many studies for thermal stress, thermal bending, and vibration of functionally graded plates are available in the literatures. Fuchiyama and Noda [1] analyzed the transient heat conduction and the thermal stress by FEM. In this work, the problem was restricted to plane strain problem and the plates were layered with homogeneous layers, that is, the change of material properties was varied in steps with the uniform homogenized material in each sub-layer. Praveen and Reddy [2] conducted the nonlinear transient thermoelastic analysis of functionally graded ceramic–metal plates using FEM. However, they were not considered the change of material properties due to temperature distribution in analysis. Loy et al. [3] presented the natural frequency of FGM cylindrical shells using theoretical method, but did not account for the effect of temperature. Becker et al. [4] investigated the thermal residual stress in FGMs, where temperature was varied only axially but material properties were constant regardless of temperature. Pradhan et al. [5] studied the vibration characteristics of FGM cylindrical shells with various boundary conditions. Ng et al. [6,7] presented the dynamic stability analysis of FGM plates and cylindrical shells under harmonic in-plane loading. Almajid et al. [8] applied the classical lamination theory to predict the out-of-plane displacement and stress field of FGM with piezoelectric layer. Yang and Shen [9] deal with the dynamic response of initially stressed FGM rectangular thin plates. Reddy and Cheng [10] investigated the free vibration of a spherical shallow shell using various shear deformation theory. The thermal effect was not considered in Refs. [5–10]. Woo and Meguid [11] provided an analytic solution for the coupled large deflection of FGM plates and shallow shells made of temperature independent materials under transverse mechanical loads and a temperature field. Shen [12] employed a mixed Galerkin-perturbation technique to analyze the nonlinear bending of FGM plates subjected to a transverse load and in uniform thermal environments. Cho and Ha [13] conducted volume fraction optimizations for minimizing the thermal stress of FGMs in a constant thermal distribution.In this study, the material properties were temperature independent and an FGM was divided into several uniform homogenized layers. Yang and Shen [14] analyzed the vibration characteristics and transient response of shear-deformable FGM plates made of temperature dependent materials in thermal environments. Also, they [15] investigated free vibration and dynamic instability of FGM cylindrical panels subjected to combined static and periodic axial forces and in thermal environment. However, they considered only uniform temperature rise through the thickness.

Reddy and Cheng [16] studied the harmonic vibration problem of functionally graded plates by means of a three-dimensional asymptotic theory formulated in terms of transfer matrix.

Many of the above-mentioned papers deal with temperature-independent materials. Some of them considered temperature dependent materials in a constant temperature field. In many cases, the temperature varies through the thickness direction if a heat flows from one surface to the other surface. In this paper, the analytical solution is provided for the vibration characteristics of FGM plates under temperature field. The temperature is assumed to be constant in the plane of the plate. The variation of temperature is assumed to occur in the thickness direction only. Two types of thermal condition are considered. The first type is that one value of the temperature is imposed on the upper surface and the other (or same) value on the lower surface. The second is that a heat flows from the upper surface to the lower one held at a prescribed temperature. Material properties are assumed to be temperature dependent, and vary continuously through the thickness according to a power law distribution in terms of the volume fractions of the constituents. The frequency equation is obtained using the Rayleigh–Ritz method based on the third-order shear deformation plate theory to account for rotary inertia and transverse shear strains. Numerical results are provided to show the effect of material compositions, plate geometry and temperature fields on the vibration characteristics.

2. Formulation

Consider an FGM rectangular plate of length a, width b and thickness h with its coordinate system (x, y, z) as shown in Fig. 1. The displacements of a plate in x, y and z directions are denoted u, v, and w, respectively. A linear elastic material behavior is considered.

2.1. Functionally graded constitute law

An FGM plate is made from a mixture of ceramics and metals, and material composition continuously varies such that the upper surface ($z = h/2$) of the plate is ceramic-rich whereas the

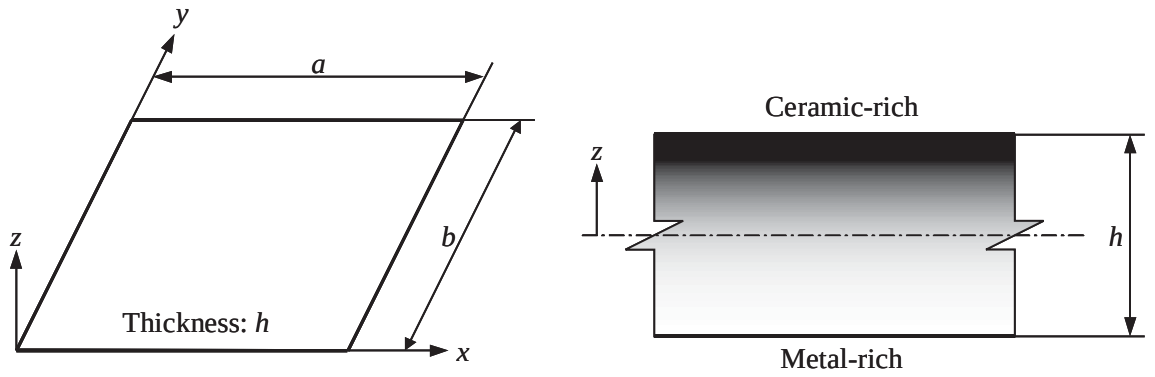

Fig. 1. Configuration of functionally graded rectangular plate.

lower surface ($z = -h/2$) is metal-rich. To obtain the effective material properties of the functionally graded plate a simple rule of mixture is adopted, i.e. a power law of type

$$P(z,T) = (P_U - P_L)\left(\frac{2z+h}{2h}\right)^p + P_L, \tag{1}$$

where P denotes a generic material property, P_L and P_U are the corresponding values at the lower and upper surfaces of the plate and p is the volume fraction index that is the positive real value. From this equation, it is notable that FGM material properties at $z = -h/2$ are same as material L. While FGM material properties at $z = h/2$ are same as those of material U. The effective material properties P are temperature dependent. A typical material property P, such as elastic modulus E, the Poisson ratio ν, mass density ρ and thermal expansion coefficient α can be expressed as a function of temperature, see Ref. [17], as

$$P = P_0(P_{-1}T^{-1} + 1 + P_1T + P_2T^2 + P_3T^3), \tag{2}$$

in which $T = T_0 + \Delta T(z)$ and $T_0 = 300\,\mathrm{K}$ (room temperature), P_0, P_{-1}, P_1, P_2 and P_3 are the coefficients of temperature T (K) and are unique to the constituent materials. $\Delta T(z)$ is temperature rise only through the thickness direction. But thermal conductivity k is temperature independent.

2.2. Governing equations

From the third-order shear deformation plate theory (TSDT) the displacement field for the considered plate may be represented by

$$\begin{aligned} u &= u_0 + z\phi_x - c_1 z^3(\phi_x + w_{0,x}),\\ v &= v_0 + z\phi_y - c_1 z^3(\phi_y + w_{0,y}),\\ w &= w_0, \end{aligned} \tag{3}$$

where u_0, v_0, w_0, ϕ_x and ϕ_y are function of x, y, t (time). u_0, v_0 and w_0 denote the displacements of a point on the middle surface and ϕ_x, ϕ_y are the rotations of a transverse normal about the y-, x-axis, respectively. A comma represents the differentiation to the space.

The in-plane and transverse shear strains are defined as

$$\begin{Bmatrix} \varepsilon_{xx} \\ \varepsilon_{yy} \\ \varepsilon_{xy} \end{Bmatrix} = \begin{Bmatrix} \varepsilon_{xx}^{(0)} \\ \varepsilon_{yy}^{(0)} \\ \varepsilon_{xy}^{(0)} \end{Bmatrix} + z\begin{Bmatrix} \varepsilon_{xx}^{(1)} \\ \varepsilon_{yy}^{(1)} \\ \varepsilon_{xy}^{(1)} \end{Bmatrix} + z^3\begin{Bmatrix} \varepsilon_{xx}^{(3)} \\ \varepsilon_{yy}^{(3)} \\ \varepsilon_{xy}^{(3)} \end{Bmatrix}, \tag{4}$$

$$\begin{Bmatrix} \gamma_{yz} \\ \gamma_{xz} \end{Bmatrix} = \begin{Bmatrix} \gamma_{yz}^{(0)} \\ \gamma_{xz}^{(0)} \end{Bmatrix} + z^2\begin{Bmatrix} \gamma_{yz}^{(3)} \\ \gamma_{xz}^{(3)} \end{Bmatrix} \tag{5}$$

and

$$\{\, \varepsilon_{xx}^{(0)} \quad \varepsilon_{yy}^{(0)} \quad \varepsilon_{xy}^{(0)} \,\} = \{\, u_{0,x} \quad v_{0,y} \quad u_{0,y} + v_{0,x} \,\}, \tag{6}$$

$$\{\, \varepsilon_{xx}^{(1)} \quad \varepsilon_{yy}^{(1)} \quad \varepsilon_{xy}^{(1)} \,\} = \{\, \phi_{x,x} \quad \phi_{y,y} \quad \phi_{x,y} + \phi_{y,x} \,\}, \tag{7}$$

$$\{\varepsilon_{xx}^{(3)} \quad \varepsilon_{yy}^{(3)} \quad \varepsilon_{xy}^{(3)}\} = -c_1\{\phi_{x,x} + w_{0,xx} \quad \phi_{y,y} + w_{0,yy} \quad \phi_{x,y} + \phi_{y,x} + 2w_{0,xy}\}, \tag{8}$$

$$\{\gamma_{xz}^{(0)} \quad \gamma_{yz}^{(0)}\} = \{w_{0,x} + \phi_x \quad w_{0,y} + \phi_y\}, \tag{9}$$

$$\{\gamma_{xz}^{(2)} \quad \gamma_{7yz}^{(2)}\} = -c_2\{w_{0,x} + \phi_x \quad w_{0,y} + \phi_y\}, \tag{10}$$

where $c_2 = 3c_1$ and $c_1 = 4/(3h^2)$.

By setting $c_1 = \gamma_{yz} = \gamma_{xz} = 0$ and replacing ϕ_x, ϕ_y by $w_{,x}$, $w_{,y}$ we recover the displacement field of the classical plate theory (CPT). The displacement field of the first-order shear deformation plate theory (FSDT) is recovered by setting $c_1 = 0$.

The stress resultants are related to the strains by the relations

$$\begin{Bmatrix} \{N\} \\ \{M\} \\ \{P\} \end{Bmatrix} = \begin{bmatrix} [A] & [B] & [E] \\ [B] & [D] & [F] \\ [E] & [F] & [H] \end{bmatrix} \begin{Bmatrix} \{\varepsilon^{(0)}\} \\ \{\varepsilon^{(1)}\} \\ \{\varepsilon^{(3)}\} \end{Bmatrix}, \quad \begin{Bmatrix} \{Q\} \\ \{R\} \end{Bmatrix} = \begin{bmatrix} [A] & [D] \\ [D] & [F] \end{bmatrix} \begin{Bmatrix} \{\gamma^{(0)}\} \\ \{\gamma^{(2)}\} \end{Bmatrix}, \tag{11}$$

$$\{N\} = \begin{Bmatrix} N_x & N_y & N_{xy} \end{Bmatrix}, \quad \{M\} = \begin{Bmatrix} M_x & M_y & M_{xy} \end{Bmatrix}, \quad \{P\} = \begin{Bmatrix} P_x & P_y & P_{xy} \end{Bmatrix}, \tag{12}$$

$$\{Q\} = \begin{Bmatrix} Q_x & Q_y \end{Bmatrix}, \quad \{R\} = \begin{Bmatrix} R_x & R_y \end{Bmatrix}, \tag{13}$$

$$\{A_{ij}, \quad B_{ij}, \quad D_{ij}, \quad E_{ij}, \quad F_{ij}, \quad H_{ij}\} = \int_{-h/2}^{h/2} Q_{ij}(1, z, z^2, z^3, z^4, z^6)\,\mathrm{d}z \quad (i,j = 1,2,6), \tag{14}$$

$$\{A_{ij}, \quad D_{ij}, \quad F_{ij}\} = \int_{-h/2}^{h/2} Q_{ij}(1, z^2, z^4)\,\mathrm{d}z \quad (i,j = 4,5). \tag{15}$$

For FSDT $A_{ij}(i,j = 4,5)$ must be modified by multiplying shear correction factor $K(= 5/6)$.

The reduced stiffness coefficients Q_{ij} are functions of z and temperature T as follows:

$$Q_{11} = Q_{22} = \frac{E(z,T)}{1 - \nu^2(z,T)}, \quad Q_{12} = \frac{\nu(z,T)E(z,T)}{1 - \nu^2(z,T)}, \quad Q_{44} = Q_{55} = Q_{66} = \frac{E(z,T)}{2[1 + \nu(z,T)]}. \tag{16}$$

The constituent relation of the plates is

$$\begin{Bmatrix} \sigma_{xx} \\ \sigma_{yy} \\ \sigma_{yz} \\ \sigma_{xz} \\ \sigma_{xy} \end{Bmatrix} = \begin{bmatrix} Q_{11} & Q_{12} & 0 & 0 & 0 \\ Q_{12} & Q_{22} & 0 & 0 & 0 \\ 0 & 0 & Q_{44} & 0 & 0 \\ 0 & 0 & 0 & Q_{55} & 0 \\ 0 & 0 & 0 & 0 & Q_{66} \end{bmatrix} \begin{Bmatrix} \varepsilon_{xx} \\ \varepsilon_{yy} \\ \gamma_{yz} \\ \gamma_{xz} \\ \varepsilon_{xy} \end{Bmatrix}. \tag{17}$$

2.3. Thermal analysis

Let us now consider the influence of a temperature filed on the behavior of the FGM. The temperature variation is assumed to occur in the thickness direction only and

one-dimensional temperature field is assumed to be constant in the plane of the plate. In this paper two types of thermal boundary condition are applied: thermal condition-I and thermal condition-II.

In thermal condition-I it is assumed that one value of the temperature is imposed on the upper surface and the other value on the lower surface. In this case, the temperature distribution along the thickness can be obtained by solving a steady-state heat transfer equation through the thickness of the plate. The equation for the temperature through the thickness is given by

$$-\frac{\mathrm{d}}{\mathrm{d}z}\left[k(z)\frac{\mathrm{d}T}{\mathrm{d}z}\right]=0, \tag{18}$$

where the thermal conductivity $k(z)$ is assumed to be independent to the temperature. This equation is solved by imposing boundary condition of $T=T_0+\Delta T_U$ at $z=h/2$ and $T=T_0+\Delta T_L$ at $z=-h/2$. The solution of this equation is

$$T(z)=T_0+\Delta T(z). \tag{19}$$

For the isotropic material plate, the temperature rise through the thickness is

$$\Delta T(z)=\frac{\Delta T_U+\Delta T_L}{2}+\frac{\Delta T_U-\Delta T_L}{h}z \tag{20}$$

and for an FGM plate,

$$\Delta T(z)=\Delta T_L+\frac{\Delta T_U-\Delta T_L}{\int_{-h/2}^{h/2}(\mathrm{d}z/k(z))}\int_{-h/2}^{z}\frac{\mathrm{d}z}{k(z)}. \tag{21}$$

In thermal condition-II it is assumed that the lower surface was held at a prescribed temperature $T_L=T_0+\Delta T_L$ and the heat flow from the upper surface to the lower one is assumed to be q (W/m^2). The heat transfer rate per unit area (heat flux) q is proportional to the normal temperature rise

$$q=-k(z)\frac{\mathrm{d}T(z)}{\mathrm{d}z}. \tag{22}$$

Solving this equation, we have the same temperature equation expressed in Eq. (19). For an isotropic material plate with constant thermal conductivity, the temperature rise through the thickness is

$$\Delta T(z)=\Delta T_L+\frac{q}{k}\left(\frac{h}{2}+\frac{q}{k}z\right). \tag{23}$$

For an FGM plate with the thermal conductivity varying through the thickness, the temperature rise through the thickness is

$$\Delta T(z)=\Delta T_L+q\int\frac{1}{k(z)}\,\mathrm{d}z. \tag{24}$$

Suppose the plate is initially stress free at temperature T_0. The plate is initially stressed by the temperature rise. The initial stresses due to temperature rise $\Delta T(z)$ are defined by

$$\begin{Bmatrix} \sigma_{xx}^{\mathrm{T}} \\ \sigma_{yy}^{\mathrm{T}} \\ \sigma_{xy}^{\mathrm{T}} \end{Bmatrix} = -\begin{bmatrix} Q_{11} & Q_{12} & 0 \\ Q_{12} & Q_{22} & 0 \\ 0 & 0 & Q_{66} \end{bmatrix} \begin{bmatrix} 1 & 0 \\ 0 & 1 \\ 0 & 0 \end{bmatrix} \begin{bmatrix} \alpha(z,T) \\ \alpha(z,T) \end{bmatrix} \Delta T(z). \tag{25}$$

2.4. Energy and frequency equation

The total strain energy of the initially stressed plate is given by

$$U = U_p + U_T, \tag{26}$$

where U_p is the strain energy due to vibratory stresses and U_T is the strain energy from the initial stresses due to temperature rise. The strain energy U_p and U_T are given by

$$U_p = \frac{1}{2}\int_V [\sigma_{xx}\varepsilon_{xx} + \sigma_{yy}\varepsilon_{yy} + \sigma_{xy}\varepsilon_{xy} + \sigma_{yz}\varepsilon_{yz} + \sigma_{xz}\varepsilon_{xz}]\,\mathrm{d}V, \tag{27}$$

$$U_T = \frac{1}{2}\int_V [\sigma_{xx}^{\mathrm{T}} d_{xx} + 2\sigma_{xy}^{\mathrm{T}} d_{xy} + \sigma_{yy}^{\mathrm{T}} d_{yy}]\,\mathrm{d}V, \tag{28}$$

$$d_{ij} = u_{,i}u_{,j} + v_{,i}v_{,j} + w_{,i}w_{,j} \quad (i,j = x,y). \tag{29}$$

The kinetic energy of the plate are given by

$$T_p = \frac{1}{2}\int_V \rho(z,T)[\dot{u}^2 + \dot{v}^2 + \dot{w}^2]\,\mathrm{d}V, \tag{30}$$

where a dot means the differentiation to the time.

The admissible displacement functions for the freely vibrating rectangular plate with any boundary conditions can be written as

$$\begin{aligned} u_0(x,y,t) &= \sum_{m=1}^{M}\sum_{n=1}^{N} \Phi_m(x)\psi_n(y)U_{mn}\cos\omega_{mn}t, \\ v_0(x,y,t) &= \sum_{m=1}^{M}\sum_{n=1}^{N} \psi_m(x)\Phi_n(y)V_{mn}\cos\omega_{mn}t, \\ w_0(x,y,t) &= \sum_{m=1}^{M}\sum_{n=1}^{N} \psi_m(x)\psi_n(y)W_{mn}\cos\omega_{mn}t, \\ \phi_x(x,y,t) &= \sum_{m=1}^{M}\sum_{n=1}^{N} \Phi_m(x)\psi_{xn}(y)X_{mn}\cos\omega_{mn}t, \\ \phi_y(x,y,t) &= \sum_{m=1}^{M}\sum_{n=1}^{N} \psi_m(x)\Phi_n(y)Y_{mn}\cos\omega_{mn}t, \end{aligned} \tag{31}$$

where $U_{mn}, V_{mn}, W_{mn}, X_{mn}$ and Y_{mn} are unknown coefficients, m and n are the half-wavenumber for x-, y-direction, and ω_{mn} is the angular natural frequency for (m, n) vibration mode. $\Phi_i(X)$ and $\psi_i(X)$ are the modal shape functions satisfying a boundary condition. The plates under consideration are clamped on all edges. The associated boundary conditions are

$$u_0 = v_0 = w_0 = w_{0,x} = \phi_x = \phi_y = 0 \quad \text{at } x \text{ edges}, \tag{32a}$$

$$u_0 = v_0 = w_0 = w_{0,y} = \phi_x = \phi_y = 0 \quad \text{at } y \text{ edges}. \tag{32b}$$

For the plate clamped at $x = 0$ and a, the modal functions $\psi_m(x)$ and $\Phi_m(x)$ using beam function can be expressed in a general form as

$$\psi_m(x) = \left(\cosh\frac{\lambda_m x}{a} - \cos\frac{\lambda_m x}{a}\right) - \sigma_i\left(\sinh\frac{\lambda_m x}{a} - \sin\frac{\lambda_m x}{a}\right), \quad \Phi_m(x) = \frac{\psi_m(x)}{\lambda_m/a}, \tag{33}$$

where the coefficient σ_m is determined from the boundary condition and λ_m does not need an integer as number depending on the wavenumber. The modal functions $\psi_n(y)$ and $\Phi_n(y)$ have the same form of $\psi_m(x)$ and $\Phi_m(x)$.

Table 1
Temperature-dependent coefficients of elastic modulus E (GPa), Poisson's ratio v, mass density ρ (kg/m^3), thermal expansion coefficient α (1/K) and thermal conductivity k (W/mK) for ceramics and metals (from Refs. [14,18])

	Material	P_{-1}	P_0	P_1	P_2	P_3
E	SUS304	0	201.04	3.079×10^{-4}	-6.534×10^{-7}	0
	Si_3N_4	0	348.43	-3.070×10^{-4}	2.160×10^{-7}	-8.946×10^{-11}
	Ti–6Al–4V	0	122.70	-4.605×10^{-4}	0	0
	ZrO_2	0	132.20	-3.805×10^{-4}	-6.127×10^{-8}	0
v	SUS304	0	0.3262	-2.002×10^{-4}	3.797×10^{-7}	0
	Si_3N_4	0	0.2400	0	0	0
	Ti–6Al–4V	0	0.2888	1.108×10^{-4}	0	0
	ZrO_2	0	0.3330	0	0	0
ρ	SUS304	0	8166	0	0	0
	Si_3N_4	0	2370	0	0	0
	Ti–6Al–4V	0	4420	0	0	0
	ZrO_2	0	3657	0	0	0
α	SUS304	0	12.330×10^{-6}	8.086×10^{-6}	0	0
	Si_3N_4	0	5.8723×10^{-6}	9.095×10^{-6}	0	0
	Ti–6Al–4V	0	7.4300×10^{-6}	7.483×10^{-4}	-3.621×10^{-7}	0
	ZrO_2	0	13.300×10^{-6}	-1.421×10^{-3}	9.549×10^{-7}	0
k	SUS304	—	—	—	—	—
	Si_3N_4	—	—	—	—	—
	Ti–6Al–4V	0	6.10	0	0	0
	ZrO_2	0	1.78	0	0	0

Substituting the displacement functions into each energy equation and then applying these results to Rayleigh–Ritz procedure, the following frequency equation is obtained:

$$[[\mathbf{K}] - \omega^2[\mathbf{M}]]\{\mathbf{P}\} = 0, \tag{34}$$

where stiffness matrix [**K**] and mass matrix [**M**] are composed of (5×5) sub-matrices and the elements of these sub-matrices are given in the appendix. Each sub-matrix of [**K**] and [**M**] matrices is of the order of $((M\times N)\times (M\times N))$. Eq. (34) is a set of linear, homogeneous and simultaneous algebraic equations. Solving this eigenvalue problem the natural frequency and its corresponding mode shape are obtained.

3. Results and discussions

Some numerical examples are now demonstrated for the present theoretical method. We consider that a FGM plate has the ceramic at the heated surface ($z = h/2$) and the metal at the cooled surface ($z = -h/2$), and their compositions vary continuously in the thickness direction of the plate. The material properties are taken into consideration the temperature dependency for the temperature range of $300\,\mathrm{K} \leqslant T \leqslant 1100\,\mathrm{K}$ as given in Table 1 from Refs. [14,18]. Type-I FGM plate, which is made of stainless steel (SUS304) on its lower surface and silicon nitride (Si_3N_4) on its upper surface, is used to validate the present method. The effect of the FGM configuration is studied by studying the frequencies of Type-II FGM plate, which is made of titanium alloy (Ti–6Al–4V) on its lower surface and zirconium oxide (ZrO_2) on its upper surface.

To validate the present method for FGM plates, the results for Type-I FGM square plates ($a = 0.2\,\mathrm{m}$) are compared with those of Yang and Shen [14], see Table 2. Also, by varying the

Table 2
Convergence and comparison study of frequency parameter $\omega^* = \omega b^2/\pi^2\sqrt{I_S/D_S}$ for Type-I FGM square plates subjected to uniform temperature rise ($p = 2.0$, $a = 0.2\,\mathrm{m}$, $a/h = 10$)

ΔT (K)	Source	Mode sequence							
		1	2	3	4	5	6	7	8
0	$M \times N = 5 \times 5$	4.1334	8.0241	8.0241	11.3513	13.2169	13.3079	16.1390	16.1390
	$M \times N = 8 \times 8$	4.1230	7.9828	7.9828	11.2457	13.1495	13.2478	16.0059	16.0059
	$M \times N = 10 \times 10$	4.1165	7.9696	7.9696	11.2198	13.1060	13.2089	15.9471	15.9471
	Ref. [14]	4.1062	7.8902	7.8902	11.1834	12.5881	13.1867	15.4530	16.0017
300	$M \times N = 5 \times 5$	3.6741	7.3587	7.3587	10.5240	12.3014	12.3964	15.0892	15.0892
	$M \times N = 8 \times 8$	3.6650	7.3217	7.3217	10.4262	12.2387	12.3410	14.9642	14.9642
	$M \times N = 10 \times 10$	3.6593	7.3098	7.3098	10.4021	12.1982	12.3052	14.9090	14.9090
	Ref. [14]	3.6636	7.2544	7.2544	10.3924	11.7054	12.3175	14.4520	15.0019
500	$M \times N = 5 \times 5$	3.2280	6.7003	6.7003	9.6892	11.3668	11.4652	14.0034	14.0034
	$M \times N = 8 \times 8$	3.2198	6.6669	6.6669	9.5986	11.3085	11.4142	13.8863	13.8863
	$M \times N = 10 \times 10$	3.2147	6.6561	6.6561	9.5761	11.2708	11.3812	13.8346	13.8346
	Ref. [14]	3.2357	6.6281	6.6281	9.5990	10.8285	11.4350	13.4412	13.9756

series number of M and N, convergence study has been undertaken in this table for the first eight natural frequency parameters $\omega^* = \omega a^2/\pi^2\sqrt{I_S/D_S}$ to arrive at the choice of suitable series numbers. D_S and I_S are chosen to be the values of D_{11} and I_0 of a stainless steel plate of $a/h = 10$ evaluated at room temperature T_0. This plate is on the uniform temperature rise. It is observed that the present method converges well enough to obtain results in good agreement with those of Ref. [14] when $M \geqslant 8$ and $N \geqslant 8$. Thus, $M \times N = 10 \times 10$ has been used in all the following computations.

In all the following computations, Type-II FGM plate, which is made of titanium alloy (Ti–6Al–4V) on its lower surface and zirconium oxide (ZrO_2) on its upper surface, is chosen. Fig. 2 presents the variation of volume fraction for ceramic, thermal conductivity and temperature field through the thickness of the FGM plate for two types of thermal condition. From Fig. 2(a), the volume fraction of ceramic V_c increases from 0 at $z = -h/2$ to 1 at $z = h/2$. At z away from $z = h/2$, the rate of decrease of V_c for $p > 1$ is high compared to $p < 1$, and z closer to $z = h/2$, the rate of increase of V_c for $p > 1$ is much higher than for $p < 1$. The non-dimensional thermal

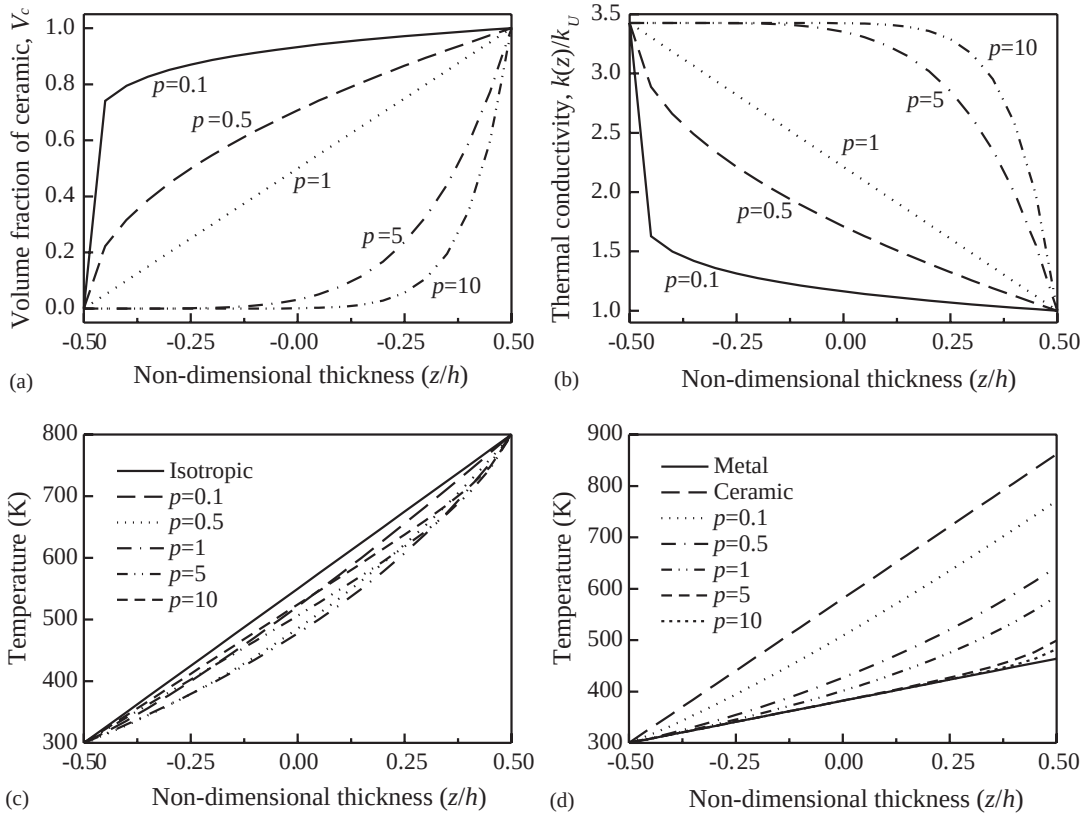

Fig. 2. Variation of volume fraction of ceramic, thermal conductivity and temperature through the non-dimensional thickness for Type-II FGM plate ($a = 0.2$ m, $a/h = 10$): (a) volume fraction of ceramic; (b) thermal conductivity; (c) temperature of thermal condition-I with $\Delta T_L = 0$ K, $\Delta T_U = 500$ K; (d) temperature of thermal condition-II with $T_L = 0$ K, $q = 5 \times 10^4$ W/m^2.

conductivity k/k_U in Fig. 2(b) decreases from k_L/k_U at $z=-h/2$ to 1 at $z=h/2$. At z away from $z=h/2$, the rate of increase of k/k_U for $p>1$ is high compared to $p<1$, and z closer to $z=-h/2$, the rate of increase of k/k_U for $p<1$ is much higher than for $p>1$. Fig. 2(c) shows the temperature distribution of plates subjected to thermal condition-I, where the upper surface is held at $T_U=800\,\mathrm{K}$ and the lower surface is held at $T_L=T_0$. For the isotropic plate subjected to this thermal type, temperature distributions are same regardless of material types as indicated in Eq. (20). It is seen that the temperature at any internal point through the thickness of the plate made of isotropic material is always higher than that corresponding to FGM plates. The temperature distribution may be almost same in case that p is close to 0 or infinite value. This is the reason that FGM is mainly composed of one isotropic material if p is close to 0 or infinite. The temperature distributions of plates subjected to thermal condition-II, where the lower surface is held at $T_L=T_0$ and the heat flow from the upper surface to the lower one is assumed to be $q=5\times10^4\,\mathrm{W/m^2}$, indicate in Fig. 2(d). The metal plate with the relatively large thermal conductivity undergoes the lowest temperature and the ceramic plate with the low thermal conductivity does the largest temperature. For the FGM plates, the temperature rise become large as the volume fraction index p decreases, i.e., the amount of the ceramic in FGM increases.

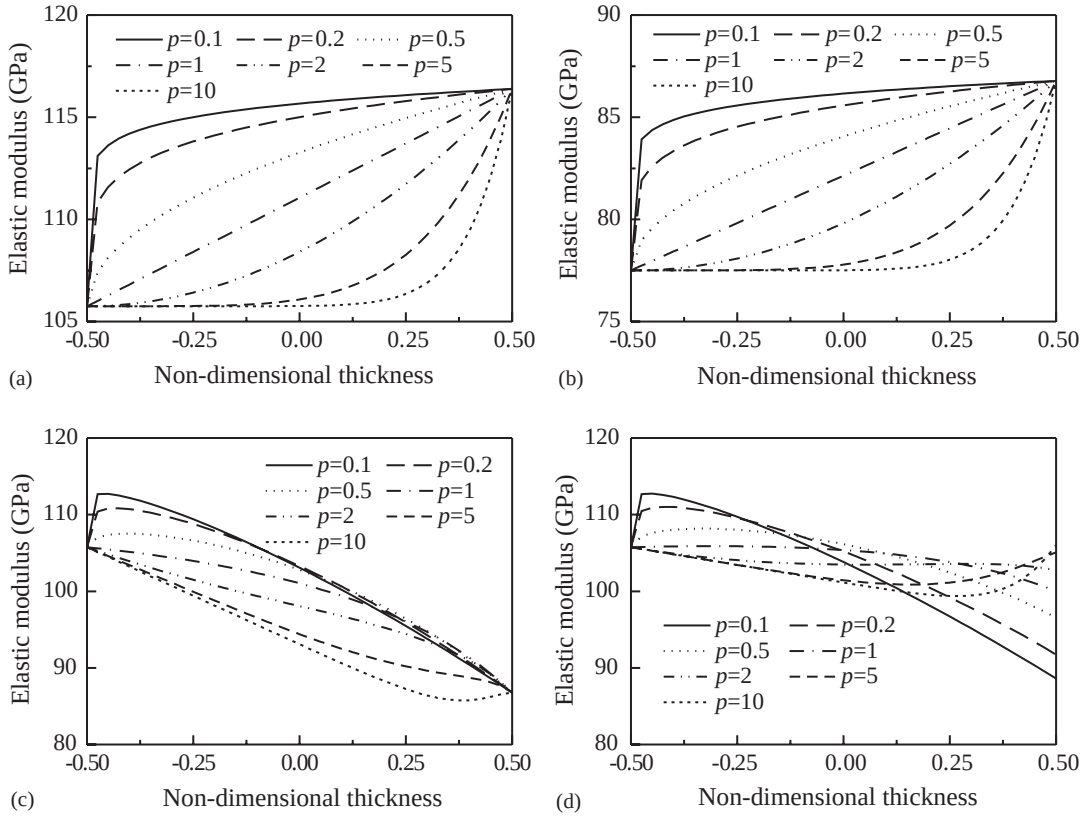

Fig. 3. Variation of elastic modulus through the non-dimensional thickness for the Type-II FGM plate ($a=0.2\,\mathrm{m}$, $a/h=10$): (a) room temperature; (b) uniform temperature rise with $\Delta T_L=\Delta T_U=500\,\mathrm{K}$; (c) thermal condition-I with $\Delta T_L=0\,\mathrm{K}$, $\Delta T_U=500\,\mathrm{K}$; (d) thermal condition-II with $\Delta T_L=0\,\mathrm{K}$, $q=5\times10^4\,\mathrm{W/m^2}$.

Fig. 3 shows the variation of elastic modulus E of FGM plates with the volume fraction index, p. Fig. 3(a) indicates elastic modulus of FGM plates on room temperature, Fig. 3(b) on uniform temperature rise with $\Delta T = 500\,\mathrm{K}$, Fig. 3(c) on thermal condition-I with $\Delta T_L = 0\,\mathrm{K}$, $\Delta T_U = 500\,\mathrm{K}$, and Fig. 3(d) on thermal condition-II with $\Delta T_L = 0\,\mathrm{K}$, $q = 5 \times 10^4\,\mathrm{W/m^2}$. For the plate on room temperature and uniform temperature environments, elastic modulus becomes large away from the lower surface according to volume of ceramic. However, elastic modulus variations of FGM plates on thermal condition-I and II are very different from those of above two cases as shown in Figs. 3(c) and (d). In thermal condition-I elastic modulus increases first, and then decreases when $p<1$. And elastic modulus decreases when $p \geqslant 1$. But elastic modulus decreases first, then increases for the large $p = 10$. For the FGM plate on thermal condition-II, elastic modulus at upper surface increases as volume fraction increases because the temperature at this surface due to heat flux becomes low as the volume fraction index increases as indicated in Fig. 2(d).

Comparison has been made between CPT, FSDT and TSDT in Table 3. The used Diff. (%) in the table is the percentage differences of CPT and FSDT results with respect to TSDT results. Compared with CPT, FSDT and TSDT results, the differences increase as a/h is decreased. This is

Table 3
Comparison study of frequency parameter $\omega^* = \omega b^2/\pi^2\sqrt{I_S/D_S}$ for Type-II FGM square plates between CPT, FSDT and TSDT ($p = 2.0$, $a = 0.2\,\mathrm{m}$, $\Delta T = 0\,\mathrm{K}$)

a/h	Source	Mode sequence							
		1	2	3	4	5	6	7	8
5	CPT	7.4122	15.1165	15.1165	20.8333	22.2877	23.6705	23.6705	24.0072
	Diff., %	33.4858	50.4234	50.4234	53.6515	45.9393	53.3123	29.4545	31.2959
	FSDT	5.5166	9.9197	9.9197	13.2982	14.8992	15.0658	17.7372	17.7372
	Diff., %	−0.6519	−1.2896	−1.2896	−1.9220	−2.4404	−2.4198	−2.9948	−2.9948
	TSDT	5.5528	10.0493	10.0493	13.5588	15.2719	15.4394	18.2848	18.2848
10	CPT	3.7063	7.5591	7.5591	11.1462	13.5517	13.6159	16.9956	16.9957
	Diff., %	9.9760	15.8430	15.8430	21.3218	26.2491	25.8715	30.1148	30.1156
	FSDT	3.3663	6.5086	6.5086	9.1503	10.6789	10.7625	12.9769	12.9769
	Diff., %	−0.1128	−0.2559	−0.2559	−0.4027	−0.5143	−0.5066	−0.6515	−0.6515
	TSDT	3.3701	6.5253	6.5253	9.1873	10.7341	10.8173	13.0620	13.0620
20	CPT	1.8531	3.7796	3.7796	5.5733	6.7762	6.8083	8.4983	8.4984
	Diff., %	2.6591	4.3368	4.3368	6.0188	7.4803	7.3763	8.8033	8.8046
	FSDT	1.8047	3.6206	3.6206	5.2524	6.2977	6.3338	7.7998	7.7998
	Diff., %	−0.0222	−0.0525	−0.0525	−0.0856	−0.1094	−0.1073	−0.1396	−0.1396
	TSDT	1.8051	3.6225	3.6225	5.2569	6.3046	6.3406	7.8107	7.8107
100	CPT	0.3706	0.7559	0.7559	1.1147	1.3553	1.3617	1.6997	1.6997
	Diff., %	0.1081	0.1723	0.1723	0.2608	0.3183	0.3168	0.3780	0.3780
	FSDT	0.3702	0.7545	0.7545	1.118	1.3509	1.3574	1.6932	1.6932
	Diff., %	0.0000	−0.0133	−0.0133	0.0000	−0.0074	0.0000	−0.0059	−0.0059
	TSDT	0.3702	0.7546	0.7546	1.1118	1.3510	1.3574	1.6933	1.6933

due to the fact that the transverse shear and rotary inertia will have more effect on a thicker plate. For the thick plates considered in this case, there is a significant difference between the results predicted by FSDT and TSDT; FSDT slightly overpredicts frequencies. The difference between the results obtained from FSDT and TSDT is insignificant for a/h ratios greater than 5.

In Table 4, we examine the vibration characteristics of the isotropic and FGM square plates in three thermal environments, i.e., uniform temperature rise of $\Delta T = 500\,\mathrm{K}$, thermal condition-I with $\Delta T_L = 0$, $\Delta T_U = 500\,\mathrm{K}$ and thermal condition-II with $\Delta T_L = 0$, $q = 5 \times 10^4\,\mathrm{W/m^2}$. In general, frequencies are the highest for the ceramic plate and lowest for the metallic plate. The frequencies increase as the volume fraction index p decrease. It is evident that the stiffness is a maximum for the ceramic plate, is a minimum for the metallic plate, and increases as the volume fraction index p decrease. On thermal condition-II, however, the frequencies of FGM plate with $p = 0.2$ are the highest. This is the reason that temperature at upper surface of this plate is much lower than that of ceramic plate due to heat flux as indicated in Fig. 2(d).

To show the effect of volume fraction index p on the fundamental frequency, the frequency ratio f/f_m for the square plate of $a/h = 5$ are plotted to material constitutions in Fig. 4, where f_m and f are the fundamental frequency of metallic plate and other plates in each temperature

Table 4
Frequency parameter $\omega^* = \omega b^2/\pi^2\sqrt{I_S/D_S}$ for Type-II FGM square plates with various thermal conditions ($a = 0.2\,\mathrm{m}$, $a/h = 10$)

Material composition	Mode sequence							
	1	2	3	4	5	6	7	8
(a) *Uniform temperature rise with* $\Delta T_L = \Delta T_U = 500\,\mathrm{K}$								
ZrO_2	3.0273	5.9890	5.9890	8.4936	9.9479	10.0318	12.1416	12.1416
FGM, $p = 0.2$	2.9224	5.7980	5.7980	8.2318	9.6467	9.7286	11.7797	11.7797
FGM, $p = 1.0$	2.7433	5.4700	5.4700	7.7800	9.1236	9.2022	11.1492	11.1492
FGM, $p = 5.0$	2.5931	5.1934	5.1934	7.3965	8.6769	8.7527	10.6091	10.6091
Ti–6Al–4V	2.4928	5.0132	5.0132	7.1522	8.3985	8.4723	10.2762	10.2762
(b) *Thermal condition-I with* $\Delta T_L = 0\,\mathrm{K}$, $\Delta T_U = 500\,\mathrm{K}$								
ZrO_2	3.3704	6.5920	6.5920	9.3125	10.8924	10.9807	13.2730	13.2730
FGM, $p = 0.2$	3.3040	6.4613	6.4613	9.1303	10.6833	10.7692	13.0201	13.0201
FGM, $p = 1.0$	3.1584	6.1792	6.1792	8.7349	10.2239	10.3058	12.4627	12.4627
FGM, $p = 5.0$	2.9970	5.8742	5.8742	8.3078	9.7238	9.8023	11.8553	11.8553
Ti–6Al–4V	2.8498	5.6098	5.6098	7.9475	9.3104	9.3865	11.3598	11.3598
(c) *Thermal condition-II with* $\Delta T_L = 0\,\mathrm{K}$, $q = 5 \times 10^4\,\mathrm{W/m^2}$								
ZrO_2	3.3242	6.5103	6.5103	9.2019	10.7654	10.8531	13.1211	13.1211
FGM, $p = 0.2$	3.3554	6.5516	6.5516	9.2522	10.8228	10.9094	13.1865	13.1865
FGM, $p = 1.0$	3.2829	6.3949	6.3949	9.0243	10.5543	10.6377	12.8558	12.8558
FGM, $p = 5.0$	3.1811	6.1887	6.1887	8.7288	10.2053	10.2856	12.4280	12.4280
Ti–6Al–4V	3.0895	6.0148	6.0148	8.4881	9.9289	10.0068	12.0946	12.0946

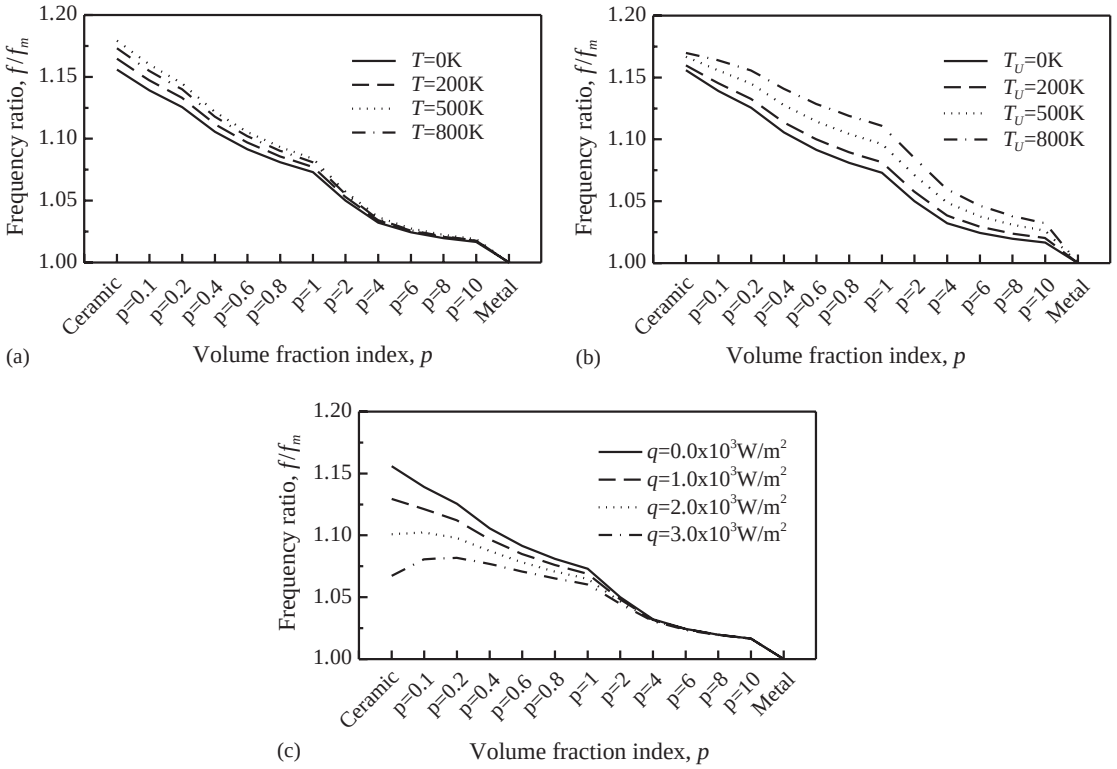

Fig. 4. Effect of volume fraction index p on the fundamental frequency of the Type-II FGM square plates ($a = 0.2$ m, $a/h = 5$, $a/b = 1$): (a) uniform temperature rise; (b) thermal condition-I with $\Delta T_L = 0$ K; (c) thermal condition-II with $\Delta T_L = 0$ K.

environment. Generally the effect of volume fraction index on high temperature environment is higher than on low temperature environment. But the effect of p in uniform temperature rise of $\Delta T = 500$ K is higher than that in $\Delta T = 800$ K because elastic modulus of metal linearly decreases and that of ceramic quadratically does with temperature. The effect of temperature for the ceramic-rich plate is higher than for the metal-rich plate on the uniform temperature rise. The effect of temperature on thermal condition-I is highest for the FGM plate of $p = 1$ and this effect decreases as p is away from 1. The effect of heat flux is very large for the ceramic-rich plate because the temperature at upper surface due to heat flux is very high compared to other material compositions. The effect of heat flux is very small for the metal-rich plate subjected to the lowest temperature field due to heat flux.

Fig. 5 gives to investigate the effect of temperature and heat flux on the fundamental frequency. Fig. 5(a) shows the frequency ratio f/f_{T0} for the square plates of $a/h = 5$ and 10 on the uniform temperature rise, where f_{T0} and f are fundamental frequencies of plates on room temperature and other temperatures. The effect of temperature for the plate of $a/h = 10$ is higher than that of $a/h = 5$ because stiffness reduction by temperature rise for $a/h = 5$ is smaller than that for $a/h = 10$. The effect of temperature becomes high as the plate becomes metal-rich. Therefore the

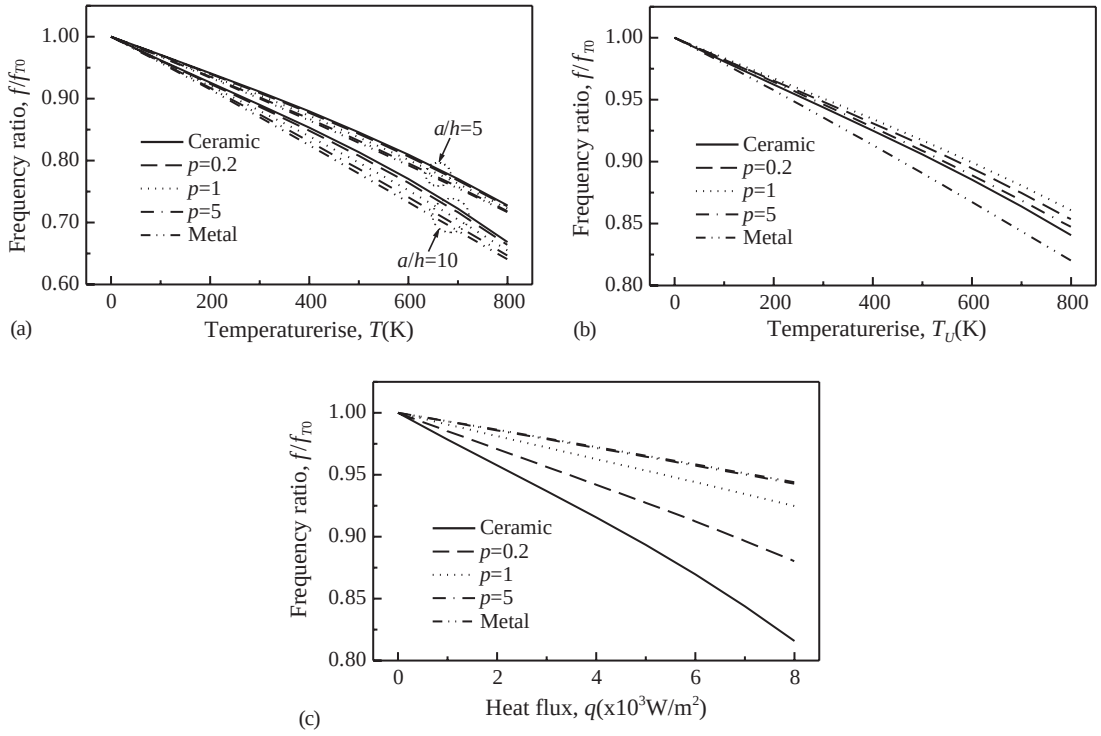

Fig. 5. Effect of temperature and heat flux on the fundamental frequency of Type-II FGM square plates ($a = 0.2$ m, $a/h = 10$): (a) uniform temperature rise; (b) thermal condition-I with $\Delta T_L = 0$ K; (c) thermal condition-II with $\Delta T_L = 0$ K.

effect is the highest for metallic plate and the lowest for ceramic plate. Fig. 5(b) and (c) present the effect of temperature and heat flux on the fundamental frequencies on thermal condition-I and II. On thermal condition-I, the effect of temperature is the highest for the metallic plate and the lowest for the FGM plate with $p = 1$. This effect for metallic plate is the higher than for the ceramic plate. This effect for isotropic plates is always higher than for FGM plates because the temperature through the thickness of FGM plate is higher for isotropic plates than for the FGM plates as indicated in Fig. 2(c). For FGM plates this effect becomes large as FGM plates becomes metal-rich or ceramic-rich. The effect for the metal-rich FGM plate is higher than that for the ceramic-rich FGM plates. The effect of heat flux becomes high as an FGM plate becomes ceramic-rich because the temperature distribution due to heat flux becomes high as the plate becomes ceramic-rich as shown in Fig. 2(d).

4. Conclusion

The temperature dependent vibration characteristics of the functionally graded rectangular plates made up of metal and ceramic are studied. The frequency equation is obtained using the

Rayleigh–Ritz procedure based on the third-order shear deformation plate theory. In theoretical formulation the initial stresses due to temperature rise are considered. The temperature is assumed to be constant in the plane of the plate. The variation of temperature is assumed to occur in the thickness direction only. Material properties are assumed to be temperature dependent, and vary continuously through the thickness according to a power law distribution in terms of the volume fractions of the constituents. The numerical results confirm that the vibration characteristics are significantly influenced by: material compositions, plate geometry and temperature rise. The present theoretical results are verified by comparing with those in literature.

Appendix

The stiffness and mass matrix [**K**], [**M**] in Eq. (34) are given as

$$[\mathbf{K}] = \begin{bmatrix} [K_{11}] & [K_{12}] & [K_{13}] & [K_{14}] & [K_{15}] \\ [K_{12}]^{\mathrm{T}} & [K_{22}] & [K_{23}] & [K_{24}] & [K_{25}] \\ [K_{13}]^{\mathrm{T}} & [K_{23}]^{\mathrm{T}} & [K_{33}] & [K_{34}] & [K_{35}] \\ [K_{14}]^{\mathrm{T}} & [K_{24}]^{\mathrm{T}} & [K_{34}]^{\mathrm{T}} & [K_{44}] & [K_{45}] \\ [K_{15}]^{\mathrm{T}} & [K_{25}]^{\mathrm{T}} & [K_{35}]^{\mathrm{T}} & [K_{45}]^{\mathrm{T}} & [K_{55}] \end{bmatrix},$$

$$[\mathbf{M}] = \begin{bmatrix} [M_{11}] & 0 & [M_{13}] & [M_{14}] & 0 \\ 0 & [M_{22}] & [M_{23}] & 0 & [M_{25}] \\ [M_{13}]^{\mathrm{T}} & [M_{23}]^{\mathrm{T}} & [M_{33}] & [M_{34}] & [M_{35}] \\ [M_{14}]^{\mathrm{T}} & 0 & [M_{34}]^{\mathrm{T}} & [M_{44}] & 0 \\ 0 & [M_{25}]^{\mathrm{T}} & [M_{35}]^{\mathrm{T}} & 0 & [M_{55}] \end{bmatrix}.$$

The elements of the sub-matrices of the stiffness matrix [**K**] and the mass matrix [**M**] are given as

$$[K_{11}]_{m\bar{m}n\bar{n}} = \frac{1}{\alpha_m \alpha_{\bar{m}}}[(A_{11} - A_{11}^{\mathrm{T}})I_{m\bar{m}n\bar{n}}^{2200} + (A_{66} - A_{22}^{\mathrm{T}})I_{m\bar{m}n\bar{n}}^{1111}],$$

$$[K_{12}]_{m\bar{m}n\bar{n}} = \frac{1}{\alpha_{\bar{m}}\beta_n}(A_{12}I_{m\bar{m}n\bar{n}}^{0220} + A_{66}I_{m\bar{m}n\bar{n}}^{1111}),$$

$$[K_{13}]_{m\bar{m}n\bar{n}} = -\frac{c_1}{\alpha_{\bar{m}}}[(E_{11} - E_{11}^{\mathrm{T}})I_{m\bar{m}n\bar{n}}^{2200} + (2E_{66} - E_{22}^{\mathrm{T}})I_{m\bar{m}n\bar{n}}^{1111} + E_{12}I_{m\bar{m}n\bar{n}}^{0220}],$$

$$[K_{14}]_{m\bar{m}n\bar{n}} = \frac{1}{\alpha_m \alpha_{\bar{m}}}[(B_{11} - c_1E_{11} - B_{11}^{\mathrm{T}} + c_1E_{11}^{\mathrm{T}})I_{m\bar{m}n\bar{n}}^{2200} + (B_{66} - c_1E_{66} - B_{22}^{\mathrm{T}} + c_1E_{22}^{\mathrm{T}})I_{m\bar{m}n\bar{n}}^{1111}],$$

$$[K_{15}]_{m\bar{m}n\bar{n}} = \frac{1}{\alpha_{\bar{m}}\beta_n}[(B_{12} - c_1E_{12})I_{m\bar{m}n\bar{n}}^{0220} + (B_{66} - c_1E_{66})I_{m\bar{m}n\bar{n}}^{1111}],$$

$$[K_{22}]_{m\bar{m}n\bar{n}} = \frac{1}{\beta_n\beta_{\bar{n}}}[(A_{22} - A_{22}^{\mathrm{T}})I_{m\bar{m}n\bar{n}}^{0022} + (A_{66} - A_{11}^{\mathrm{T}})I_{m\bar{m}n\bar{n}}^{1111}],$$

$$[K_{23}]_{m\bar{m}n\bar{n}} = -c_1[E_{12}I_{m\bar{m}n\bar{n}}^{2002} + (2E_{66} - E_{11}^{\mathrm{T}})I_{m\bar{m}n\bar{n}}^{1111} + (E_{22} - E_{22}^{\mathrm{T}})I_{m\bar{m}n\bar{n}}^{0022}],$$

$$[K_{24}]_{m\bar{m}n\bar{n}} = -\frac{1}{\alpha_m\beta_{\bar{n}}}[(B_{12} - c_1E_{12})I_{m\bar{m}n\bar{n}}^{2002} + (B_{66} - c_1E_{66})I_{m\bar{m}n\bar{n}}^{1111}],$$

$$[K_{25}]_{m\bar{m}n\bar{n}} = \frac{1}{\beta_n\beta_{\bar{n}}}[(B_{22} - c_1E_{22} - B_{22}^{\mathrm{T}} + c_1E_{22}^{\mathrm{T}})I_{m\bar{m}n\bar{n}}^{0022} + (B_{66} - c_1E_{66} - B_{11}^{\mathrm{T}} + c_1E_{11}^{\mathrm{T}})I_{m\bar{m}n\bar{n}}^{1111}],$$

$$\begin{aligned}[K_{33}]_{m\bar{m}n\bar{n}} = {} & (A_{55} - 6c_1D_{55} + 9c_1^2F_{55} - A_{11}^{\mathrm{T}})I_{m\bar{m}n\bar{n}}^{1100} + (A_{44} - 6c_1D_{44} + 9c_1^2F_{44} - A_{22}^{\mathrm{T}})I_{m\bar{m}n\bar{n}}^{0011} \\ & + c_1^2(H_{11} - H_{11}^{\mathrm{T}})I_{m\bar{m}n\bar{n}}^{2200} + c_1^2H_{12}(I_{m\bar{m}n\bar{n}}^{0220} + I_{m\bar{m}n\bar{n}}^{2002}) + c_1^2(H_{22} - H_{22}^{\mathrm{T}})I_{m\bar{m}n\bar{n}}^{0022} \\ & + c_1^2(4H_{66} - H_{11}^{\mathrm{T}} - H_{22}^{\mathrm{T}})I_{m\bar{m}n\bar{n}}^{1111},\end{aligned}$$

$$\begin{aligned}[K_{34}]_{m\bar{m}n\bar{n}} = {} & \frac{1}{\alpha_m}[(A_{55} - 6c_1D_{55} + 9c_1^2F_{55})I_{m\bar{m}n\bar{n}}^{1100} + (c_1^2H_{11} - c_1F_{11} - c_1^2H_{11}^{\mathrm{T}} + c_1F_{11}^{\mathrm{T}})I_{m\bar{m}n\bar{n}}^{2200} \\ & + (c_1^2H_{12} - c_1F_{12})I_{m\bar{m}n\bar{n}}^{2002} + (2c_1^2H_{66} - 2c_1F_{66} - c_1^2H_{22}^{\mathrm{T}} + c_1F_{22}^{\mathrm{T}})I_{m\bar{m}n\bar{n}}^{1111}],\end{aligned}$$

$$\begin{aligned}[K_{35}]_{m\bar{m}n\bar{n}} = {} & \frac{1}{\beta_n}[(A_{44} - 6c_1D_{44} + 9c_1^2F_{44})I_{m\bar{m}n\bar{n}}^{0011} + (c_1^2H_{22} - c_1F_{22} - c_1^2H_{22}^{\mathrm{T}} + c_1F_{22}^{\mathrm{T}})I_{m\bar{m}n\bar{n}}^{0022} \\ & + (c_1^2H_{12} - c_1F_{12})I_{m\bar{m}n\bar{n}}^{0220} + (2c_1^2H_{66} - 2c_1F_{66} - c_1^2H_{11}^{\mathrm{T}} + c_1F_{11}^{\mathrm{T}})I_{m\bar{m}n\bar{n}}^{1111}],\end{aligned}$$

$$\begin{aligned}[K_{44}]_{m\bar{m}n\bar{n}} = {} & \frac{1}{\alpha_m\alpha_{\bar{m}}}[(D_{11} - 2c_1F_{11} + c_1^2H_{11} - D_{11}^{\mathrm{T}} - c_1^2H_{11}^{\mathrm{T}} + 2c_1F_{11}^{\mathrm{T}})I_{m\bar{m}n\bar{n}}^{2200} \\ & + (D_{66} - 2c_1F_{66} + c_1^2H_{66} - D_{22}^{\mathrm{T}} - c_1^2H_{22}^{\mathrm{T}} + 2c_1F_{22}^{\mathrm{T}})I_{m\bar{m}n\bar{n}}^{1111} \\ & + (A_{55} - 6c_1D_{55} + 9c_1^2F_{55})I_{m\bar{m}n\bar{n}}^{1100}],\end{aligned}$$

$$[K_{45}]_{m\bar{m}n\bar{n}} = \frac{1}{\alpha_{\bar{m}}\beta_n}[(D_{12} - 2c_1F_{12} + c_1^2H_{12})I_{m\bar{m}n\bar{n}}^{0220} + (D_{66} - 2c_1F_{66} + c_1^2H_{66})I_{m\bar{m}n\bar{n}}^{1111}],$$

$$\begin{aligned}[K_{55}]_{m\bar{m}n\bar{n}} = {} & \frac{1}{\beta_n\beta_{\bar{n}}}[(D_{22} - 2c_1F_{22} + c_1^2H_{22} - D_{22}^{\mathrm{T}} - c_1^2H_{22}^{\mathrm{T}} + 2c_1F_{22}^{\mathrm{T}})I_{m\bar{m}n\bar{n}}^{0022} \\ & + (D_{66} - 2c_1F_{66} + c_1^2H_{66} - D_{11}^{\mathrm{T}} - c_1^2H_{11}^{\mathrm{T}} + 2c_1F_{11}^{\mathrm{T}})I_{m\bar{m}n\bar{n}}^{1111} \\ & + (A_{44} - 6c_1D_{44} + 9c_1^2F_{44})I_{m\bar{m}n\bar{n}}^{0011}],\end{aligned}$$

$$[M_{11}]_{m\bar{m}n\bar{n}} = \frac{I_0I_{m\bar{m}n\bar{n}}^{1100}}{\alpha_m\alpha_{n\bar{n}}}, \quad [M_{13}]_{m\bar{m}n\bar{n}} = -\frac{c_1I_3I_{m\bar{m}n\bar{n}}^{1100}}{\alpha_{n\bar{n}}}, \quad [M_{14}]_{m\bar{m}n\bar{n}} = \frac{(I_1 - c_1I_3)I_{m\bar{m}n\bar{n}}^{1100}}{\alpha_m\alpha_{n\bar{n}}},$$

$$[M_{22}]_{m\bar{m}n\bar{n}} = \frac{I_0I_{m\bar{m}n\bar{n}}^{0011}}{\beta_n\beta_{\bar{n}}}, \quad [M_{23}]_{m\bar{m}n\bar{n}} = -\frac{c_1I_3I_{m\bar{m}n\bar{n}}^{0011}}{\beta_{\bar{n}}}, \quad [M_{25}]_{m\bar{m}n\bar{n}} = \frac{(I_1 - c_1I_3)I_{m\bar{m}n\bar{n}}^{0011}}{\beta_n\beta_{\bar{n}}},$$

$$[M_{33}]_{m\bar{m}n\bar{n}} = I_1 I^{0000}_{m\bar{m}n\bar{n}} - c_1^2 I_6 (I^{1100}_{m\bar{m}n\bar{n}} + I^{0011}_{m\bar{m}n\bar{n}}), \quad [M_{34}]_{m\bar{m}n\bar{n}} = \frac{c_1(c_1 I_6 - I_4) I^{1100}_{m\bar{m}n\bar{n}}}{\alpha_m},$$

$$[M_{35}]_{m\bar{m}n\bar{n}} = \frac{c_1(c_1 I_6 - I_4) I^{0011}_{m\bar{m}n\bar{n}}}{\beta_n},$$

$$[M_{44}]_{m\bar{m}n\bar{n}} = \frac{(I_2 - 2c_1 I_4 + c_1^2 I_6) I^{1100}_{m\bar{m}n\bar{n}}}{\alpha_m \alpha_{\bar{n}}}, \quad [M_{55}]_{m\bar{m}n\bar{n}} = \frac{(I_2 - 2c_1 I_4 + c_1^2 I_6) I^{0011}_{m\bar{m}n\bar{n}}}{\beta_n \beta_{\bar{n}}},$$

where

$$\alpha_i = \frac{\lambda_i}{a}, \quad \beta_i = \frac{\lambda_i}{b}, \quad I^{pqrs}_{m\bar{m}n\bar{n}} = \int_0^L \frac{\partial^{(p)}\psi_m}{\partial x^{(p)}} \frac{\partial^{(q)}\psi_{\bar{m}}}{\partial x^{(q)}} \, \mathrm{d}x \int_0^b \frac{\partial^{(r)}\psi_n}{\partial y^{(r)}} \frac{\partial^{(s)}\psi_{\bar{n}}}{\partial y^{(s)}} \, \mathrm{d}y,$$

$$\{A^{\mathrm{T}}_{ii}, B^{\mathrm{T}}_{ii}, D^{\mathrm{T}}_{ii}, E^{\mathrm{T}}_{ii}, F^{\mathrm{T}}_{ii}, H^{\mathrm{T}}_{ii}\} = \int_{-h/2}^{h/2} \sigma_i^{\mathrm{T}}(1, z, z^2, z^3, z^4, z^6) \, \mathrm{d}z \quad (i = 1, 2; x, y \text{ for } \sigma_i^{\mathrm{T}}),$$

$$\{I_0, I_1, I_2, I_3, I_4, I_6\} = \int_{-h/2}^{h/2} \rho(z)(1, z, z^2, z^3, z^4, z^6) \, \mathrm{d}z \quad (i, j = 1, 2, 6).$$

References

[1] T. Fuchiyama, N. Noda, Analysis of thermal stress in a plate of functionally gradient material, *JSAE Review* 16 (1995) 263–268.

[2] G.N. Praveen, J.N. Reddy, Nonlinear transient thermoelastic analysis of functionally graded ceramic-metal plates, *International Journal of Solids and Structures* 35 (1998) 4457–4476.

[3] C.T. Loy, K.Y. Lam, J.N. Reddy, Vibration of functionally graded cylindrical shells, *International Journal of Mechanical Sciences* 41 (1999) 309–324.

[4] T.L. Becker, R.M. Cannon, R.O. Ritchie, An approximate method for residual stress calculation in functionally graded materials, *Mechanics of Materials* 32 (2000) 85–97.

[5] S.C. Pradhan, C.T. Loy, K.Y. Lam, J.N. Reddy, Vibration characteristics of functionally graded cylindrical shells under various boundary conditions, *Applied Acoustics* 61 (2000) 111–129.

[6] T.Y. Ng, K.Y. Lam, K.M. Liew, Effects of FGM materials on the parametric resonance of plate structures, *Computer Methods in Applied Mechanics and Engineering* 190 (2000) 953–962.

[7] T.Y. Ng, K.Y. Lam, K.M. Liew, J.N. Reddy, Dynamic stability analysis of functionally graded cylindrical shells under periodic axial loading, *International Journal of Solids and Structures* 38 (2001) 1295–1309.

[8] A. Almajid, M. Taya, S. Hudnut, Analysis of out-of-plane displacement and stress field in a piezocomposite plate with functionally graded microstructure, *International Journal of Solids and Structures* 38 (2001) 3377–3391.

[9] J. Yang, H.S. Shen, Dynamic response of initially stressed functionally graded rectangular thin plates, *Composite Structures* 54 (2001) 497–508.

[10] J.N. Reddy, Z.Q. Cheng, Frequency correspondence between membranes and functionally graded spherical shallow shells of polygonal planform, *International Journal of Mechanical Sciences* 44 (2002) 967–985.

[11] J. Woo, S.A. Meguid, Nonlinear analysis of functionally graded plates and shallow shells, *International Journal of Solids and Structures* 38 (2001) 7409–7421.

[12] H.S. Shen, Nonlinear bending response of functionally graded plates subjected to transverse loads and in thermal environments, *International Journal of Mechanical Sciences* 44 (2002) 561–584.

[13] J.R. Cho, D.Y. Ha, Volume fraction optimization for minimizing thermal stress in Ni–Al_2O_3 functionally graded materials, *Materials Science and Engineering A* 334 (2002) 147–155.

[14] J. Yang, H.S. Shen, Vibration characteristics and transient response of shear-deformable functionally graded plates in thermal environments, *Journal of Sound and Vibration* 255 (2002) 579–602.
[15] J. Yang, H.S. Shen, Free vibration and parametric resonance of shear deformable functionally graded cylindrical panels, *Journal of Sound and Vibration* 261 (2003) 871–893.
[16] J.N. Reddy, Z.Q. Cheng, Frequency of functionally graded plates with three-dimensional asymptotic approach, *Journal of Engineering Mechanics* 129 (2003) 896–900.
[17] Y.S. Touloukian, *Thermophysical Properties of High Temperature Solid Materials*, MacMillan, New York, 1967.
[18] Y. Ootao, R. Kawamura, Y. Tanigawa, R. Imamura, Optimization of material composition of nonhomogeneous hollow sphere for thermal stress relaxation making use of neural network, *Computer Methods in Applied Mechanics and Engineering* 180 (1999) 185–201.